Heliyon 8 (2022) e09610

Contents lists available at ScienceDirect

Heliyon

journal homepage: www.cell.com/heliyon

Research article

Adsorption kinetics and isotherms of binary metal ion aqueous solution using untreated venus shell

Attaso Khamwichit [a,b], Wipawee Dechapanya [a,b,*], Wipada Dechapanya [c]

[a] School of Engineering and Technology, Walailak University, 222 Thaiburi, Thasala, Nakhon Si Thammarat, 80160, Thailand
[b] Excellent Research Center of Palm Oil and Biomass, Walailak University, 222 Thaiburi, Thasala, Nakhon Si Thammarat, 80160, Thailand
[c] Faculty of Engineering, Ubon Ratchathani University, 85 Sathonlamark Rd. Mueang Si Khai, Warin Chamrap, Ubon Ratchathani, 34190, Thailand

GRAPHICAL ABSTRACT

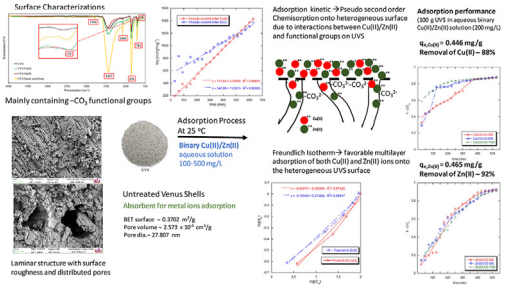

ARTICLE INFO

Keywords:
Heavy metal
Adsorption isotherm
Biosorption
Adsorption modeling
Venus shell
Waste utilization

ABSTRACT

Among available technologies to remove heavy metals from wastewater, biosorption has gained more attention due to its high removal efficiency, friendly operation, and inexpensive cost. Despite many studies on metal adsorption from single ion solutions, kinetics and isotherms of binary metal ions simultaneously adsorbed onto biosorbents have not been thoroughly investigated to provide insight on involving mechanisms. This study explored the adsorption potential of untreated venus shells (UVS) that can be utilized in economical and environmentally-friendly ways. In this work, UVS of different sizes were prepared without chemical treatment as a biosorbent. Characterization of UVS was accomplished using nitrogen adsorption isotherm, FTIR, and SEM-EDX. Batch adsorption was carried out to study the effect of initial metal ion concentration, adsorbent dosage, and size on removing Cu(II) and Zn(II) from a binary solution of both metal ions using UVS. The experimental values of maximum adsorption capacities of Cu(II) and Zn(II) were 0.446 and 0.465 mg/g, respectively. The adsorption data were analyzed using the pseudo-first order, pseudo-second order, Elovich, and intraparticle diffusion rate equations. The pseudo-second order and the intraparticle diffusion model yielded the best fit to the experimental data for Cu(II) and Zn(II) ions, respectively. The equilibrium isotherm was examined using the Langmuir, Freundlich, Temkin, Dubinin–Radushkevich (D–R), and Elovich models. The Freundlich model best fits the Cu(II) and Zn(II) equilibrium adsorption data. The results indicated that the adsorption of Cu(II) and Zn(II) onto UVS-600 adsorbent could undergo a chemisorption mechanism. Both metal ions in an aqueous solution were competitively adsorbed onto the heterogeneous active sites available on the shell surfaces. Cu(II) and Zn(II) ions in the binary system could result in ionic interference between the adsorbed ions and the active sites.

* Corresponding author.
E-mail addresses: khamwipawee@gmail.com, kwipawee@wu.ac.th (W. Dechapanya).

https://doi.org/10.1016/j.heliyon.2022.e09610
Received 8 February 2022; Received in revised form 2 March 2022; Accepted 26 May 2022

1. Introduction

Contamination of heavy metals in water resources from industrial wastewater induces problems involving several aspects such as human health and the aquatic environment [1]. This issue has risen rapidly and with the rapid growth of industrialization over the past decades. Heavy metal contamination in wastewater, primarily from industrial effluent, has become a significant concern of water pollution [2]. Contaminated heavy metal discharging into natural water reservoirs arose from various industries, including mining, smelting, refining ores, fertilizer industries, electric board manufacturing, tanneries, batteries, and paper industries [3]. Typically, these heavy metals are highly water-soluble, toxic, and carcinogenic, harmful to humans and aquatic lives [4].

The release of several toxic metals into the environment from industrial wastewater and other human activities occurs both directly and indirectly. These pollutants, unlike organic contaminants, are not biodegradable and can travel up the food chain via bioaccumulation [5]. Roughly twenty heavy metals are classified as toxic, and half of them potentially pose a risk to human health and aquatic lives [2]. Some metals, including zinc and copper, are micronutrients for most organisms; however, when the concentrations in the environment are very high, they become more toxic [3, 5, 6, 7]. The divalent of copper (Cu(II)), in the more stable form, is carcinogenic and considered to be toxic to health through ingestion of high doses [3]. Acute symptoms of toxic dose exposure of copper include liver damage, Wilson disease, and insomnia [2]. Zinc is relatively non-toxic to human health compared to cadmium, lead, or copper; nevertheless, exposure to the high dosage of zinc can lead to acute zinc intoxication [8]. These symptoms, abdominal pain, nausea, vomiting, lethargy, anemia, dizziness, depression, lethargy, neurological signs, and nervous system possibly arise from the digestion of toxic dose of zinc [2, 9]. The MCL standards of Cu(II) and Zn(II) are 0.25 and 0.80 mg/L, respectively [10].

There are a variety of physical and chemical processes to remove heavy metals from wastewater streams, such as ultra-filtration, electrochemical precipitation, chelation, ion exchange, reverse osmosis, and electrodialysis [11, 12]. Drawbacks of chemical processes include the high cost of chemicals used, high-energy consumption, toxic sludge disposal, and less efficiency than a physical process. Adsorption has been widely used over the years because of its rather high efficiency, easy operation, relatively inexpensive, and reversibility and desorption capability [13, 14]. Aside from the elimination of heavy metals, adsorption is regularly used for dye removal [14, 15]. However, the cost of the adsorption process is mainly related to the adsorbent. Some adsorbent provides high efficiency but is costly such as commercial activated carbon (CAC). Therefore, the reuse of agro/food wastes material as biosorbents for the removal of metal ions in wastewater is an emerging and potentially alternative method [16]. Biomaterials that are abundantly available as agricultural or food wastes have great potential to be used as a biosorbent because they are economical and environmentally friendly [17, 18, 19]. It was estimated that approximately one-third of the food consumption worldwide became wastes each year [20]; thus, utilization of various food wastes as biosorbents not only turns wastes into value-added products but also minimizes the food waste amounts. Biosorption capacities of various agro/food wastes, such as wheat bran [21], rice husk [22], and potato peel ($ZnCl_2$ treated) [23], for the removal of Cu(II) ion were in the range of 8.34–74.0 mg/g. While biosorption capacities of Zn(II) using various adsorbents, including tea waste [24], Cicerarientinumseed [25], mango peel [26], varied from 16.4 to 28.2 mg/g. Utilization of a variety of shells, namely fresh mussel shells [27], apple snail shells [28], oyster shells [29], and calcite mollusk shells [30], yielded biosorption capacities of 0.45–81.3 mg/g in Cd(II) reduction.

Recently, sea materials have gained attention among other natural materials to be exploited as a biosorbent regarding their high adsorption capacity, affordability, availability, waste utilization, and eco-friendly [31, 32]. Nonetheless, understanding the adsorption capability, kinetic, and isotherm of heavy metal removal using UVS is not profoundly explored. In addition, most previous studies involving the adsorption of heavy metals in an aqueous solution focus only on the removal of mono metal ions for each treatment [33, 34]. Therefore, the purpose of this study is to apply UVS, profusely found as consumed wastes in the Southern region of Thailand, as a low-cost biosorbent to remove Cu(II) and Zn(II) ions from aqueous solution. The shell was used without the chemical pretreatment regarding cost minimization. The essential factors, including adsorbent dose, initial metal ion concentration, and adsorbent size, were investigated to study the effect of these ions combinations in aqueous solution on adsorption mechanisms. Four kinetic models and six isotherm models were examined in this study. The results from a batch system on the study on their adsorption kinetics and isotherm onto the shells would give a better understanding of involving adsorption mechanisms and insights on potential applications in wastewater treatment. The implications of this study would offer the novelty challenges and opportunities of food waste eco-recycling in the biosorption process for the eradication of mixed metal ions from wastewater effluents.

2. Materials and methods

2.1. Venus shell adsorbent preparation

Venus shells, primarily used in food industries, can be lavishly found as wastes with no economic value in the Southern region of Thailand. In this study, grounded venus shells were obtained from a factory in Surat Thani province. The shell covers were washed with tap water, followed by washing with deionized water. After that, the venus shells were heated at 110 °C for 24 h. After drying, venus shells were meshed using a stable arm grinder. Dried-fine venus shells were segregated by sieve tray into three different size ranges: 300–599, 600–1179, and bigger than 1180 microns for the adsorption studies.

2.2. Characterization of venus shell adsorbents

Chemical and physical characterization of UVS adsorbents was analyzed as the following elaboration. The external and internal surfaces and structures were examined using Scanning electron microscopy (SEM) equipped with energy dispersive X-ray analysis (EDX) in Zeiss Merlin VP compact, Germany, operated at 5 and 10 kV for image scanning and electron mapping, respective. Pore properties and BET surface areas of UVS were analyzed via nitrogen adsorption-desorption isotherm at 77 K (ASAP2460, Micromeritics, USA). In BET analysis, the samples were degassed at 80 °C for 5 h. Functional groups of UVS were assessed by Fourier-transform infrared (FTIR) spectroscopy (TENSOR 27, Bruker) recorded in the wavelength of 500–4000 cm^{-1} with a resolution of 2.0 cm^{-1}.

2.3. Preparation of metal solution

All used reagents and chemicals in this study were commercial-grade, purchased from Sigma Aldrich. Commercial $ZnSO_3$ and $CuSO_3$ standards of 1000 mg/L were dissolved in distilled water to obtain the desired concentration of ions in the aqueous solution. The addition of 0.1 M NaOH was used to adjust the pH of the solution to the pH value of 7.

2.4. Experimental setup for batch studies

For the batch experiments of heavy metal removal using the UVS adsorbent, Cu(II) and Zn(II) were selected for this study. UVS was varied in the range of 0.25–10 g to study the effect of its dosage on the sorption process. The initial binary metal ion concentration of 400 mg/L, adsorbent size of 600–1170 micron, and contact time of 2880 min were applied in this set of experiments. The amount of 250 mL binary metal ion solution of 400 mg/L of initial concentrations was prepared in a

500-ml beaker. Then various amounts of UVS, in the range as mentioned earlier, were added into beakers. During the batch experiments, the solutions were shaken continuously at the rotational speed of 100 rpm using a shaking incubator. At each 30 min interval, the shaker was interrupted, and 5 ml of solution was sampled and filtered by using filtering paper (NO. 1). The clear solution was analyzed for Cu(II) and Zn(II) concentrations using Inductively Coupled Plasma, Optical Emission Spectroscopy (ICP-OES), PerkinElmer Avio200, USA.

After determination of adsorbent dosage impact on adsorption process, the effect of adsorbent size was as well investigated. However, with the exhibition of adsorbent dosage results, the fixed parameters of the second set of the experiments comprised of 100 g of adsorbent used, 720 min contacting time, and initial ion concentration of 200 mg/L While the adsorbent size was varied in the range of 300–599, 600–1179, and bigger than 1180 microns.

2.5. Modeling of batch adsorption of Zn(II) and Cu(II) ions

The adsorption capacity (amount of metal ions adsorbed in milligram per gram) was determined using the mass balance equation, as shown in Eq. (1):

$$q_e = \frac{(C_0 - C_e)V}{m} \quad (1)$$

where q_e is the amount of ion adsorbed onto adsorbent in the unit of mg/g, C_o is initial ion concentration in solution (mg/L), C_e is equilibrium metal ion concentration (mg/L), V is a volume of aqueous solution (L), and m is an adsorbent amount (g). Metal ion removal efficiency is calculated from Eq. (2):

$$removal = \frac{(C_o - C)}{C_o} \quad (2)$$

where C is ion concentration in the solution at time t.

For the adsorption kinetic and isotherm investigation, the UVS with an average size of 600–1170 microns was utilized. Initial ion concentration was varied from 100, 200, 300, 400, and 500 mg/L. The pH of the ion solution was adjusted to a value of 7. Four kinetic models, namely pseudo-first order (PFO), pseudo-second order (PSO), Elovich, and the Intraparticle diffusion model, were examined. For the adsorption isotherm analysis, the equilibrium concentration was employed to fit with the Langmuir, Freundlich, Dubinin-Radushkevich, Temkin, and Elovich.

3. Results and discussion

3.1. Characterization of venus shell adsorbents

The surface properties of UVS samples, as shown in Figure 1, were characterized. The results of BET specific surface area, pore volume, and average pore size of the untreated venus shells (UVS) are summarized in Table 1.

Table 1. Surface properties of untreated venus shells.

Sample	Description	BET surface area (m^2/g)	Pore volume ($\times 10^3$ cm^3/g)	Mean pore diameter (nm)
UVS-300	Untreated venus shells with average size 300–600 μm	0.4729	3.151	26.654
UVS-600	Untreated venus shells with average size 600 -1,800 μm	0.3702	2.573	27.807
UVS-1180	Untreated venus shells with average size greater than 1,180 μm	0.1886	1.901	28.314

Reducing the adsorbent size by physical grinding of the UVS resulted in the increased specific surface area and pore volume but insignificantly unaffected the pore diameter. The UVS-300 sample (untreated shells with the average size of 300–600 μm) gave the highest values of specific surface area (0.4729 m^2/g) and pore volume (3.15×10^{-3} cm^3/g), followed by those of the UVS-600 and UVS-1180, respectively. The specific surface areas of UVS from this study are in the range of that of freshwater snail shells (<2 m^2/g) [13]. The average pore diameters of the three samples were found to be relatively indifferent, and the values were in the range of 26.654–28.314 nm. These surface properties, including surface area, pore volume, and porosity, are important factors that influent the adsorption of Cu(II) and Zn(II) ions onto the adsorbent [35].

Since the size of different sizes of UVS exhibited indifference in morphology; thus, the scanning image of UVS-600 is presented as representative of the three sized UVS. The SEM micrographs of UVS-600 are illustrated in Figure 2. The results revealed the morphology of the UVS featuring the laminar structure with some degree of surface roughness due to the deposited materials. The morphological characteristics (e.g., surface structure) of the UVS were similar to those of the absorbent shells reported in the other studies [36, 37, 38]. The dispersed tubular holes were also observed on the UVS surface.

The element analysis of the UVS samples was taken from the EDX result, as illustrated in Figure 3. The UVS mainly consisted of O (43.1 wt %), Ca (44.4wt%), C (12.1 wt%), and Si (0.4 wt%) elements. In comparison, the samples after adsorption by metal ions showed traced amount of corresponding Cu(II) and Zn(II) being adsorbed, as summarized in Table 2. The EDX results were in good agreement with related studies reported elsewhere [13, 36]. The elemental mapping results of the UVS samples before and after adsorption is presented in Figure 4. After adsorption, Both Cu(II) and Zn(II) were according adsorbed by active sites presented on the UVS surfaces. However, EDX spectra are associated with elemental mapping generated by SEM, which is performed at a certain position on the surface of materials. Since the UVS samples are heterogeneous, elemental compositions could be different depending on the positions of the taken SEM images.

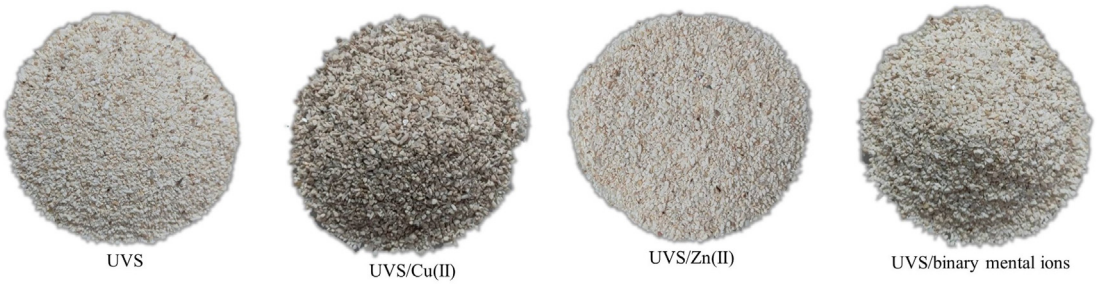

Figure 1. Untreated Venus shell (UVS) samples (from left to right): before adsorption, after adsorption with Cu(II), after adsorption with Zn(II), and after adsorption with binary Cu(II)/Zn(II).

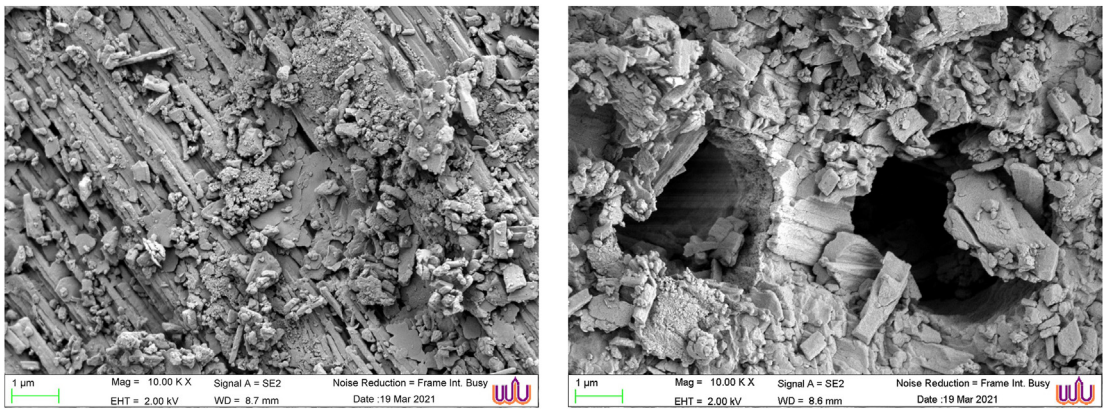

Figure 2. SEM results of untreated venus shells (UVS-600).

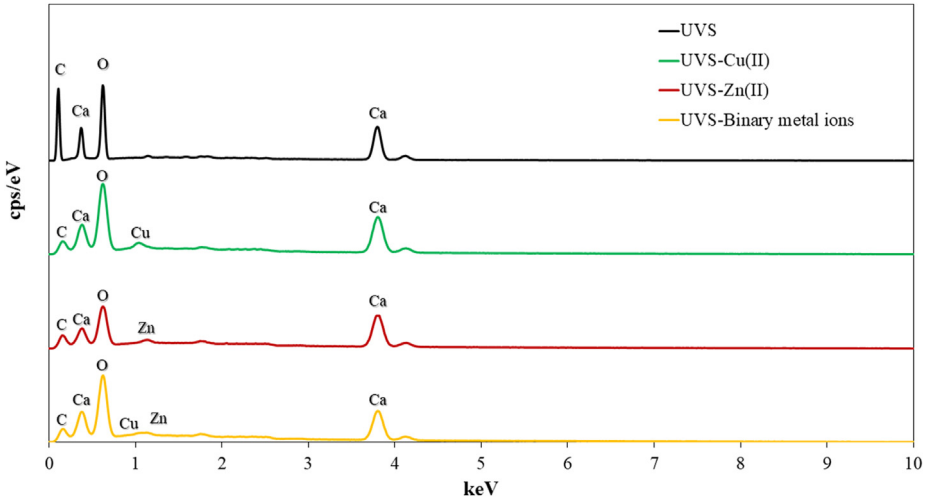

Figure 3. EDX Spectra of UVS-600 samples before and after being adsorbed by metal ions.

Table 2. EDX elemental analysis summary.

Sample	C (wt %)	O (wt %)	Ca (wt %)	Cu (wt %)	Zn (wt %)	Si (wt %)
UVS	12.1	43.1	44.4	-	-	0.4
UVS-Cu (II)	15.5	49.3	31.1	3.8	-	0.3
UVS-Zn (II)	15.2	45.3	37.3	-	2.1	0.1
UVS-binary Cu(II)/ Zn(II)	17.9	50.3	28.6	1.4	1.7	0.1

Figure 5 shows the FTIR result of UVS before and after adsorption of Cu(II), Zn(II), and binary Cu(II)/Zn(II) using 100 g of adsorbent at the initial metal ion concentration of 200 mg/L each. The results revealed that the chemical structure of the UVS mainly contained carbonate ($–CO_3$) functional groups. The bands at 711, 856, and 1437 cm^{-1} correspond to the vibration modes of C–O bonds: asymmetric stretching ($\nu 3$), out-of-plane bending ($\nu 2$), and in-plane bending ($\nu 4$), respectively, while the band at 1784 cm^{-1} is associated with harmonic vibrations [38]. The $–CO_3$ groups were presented in both calcite and aragonite phases. Aragonite exhibited characteristic peak at 1081 cm^{-1} (symmetric stretching) and 856 cm^{-1} (out-of-plane bending) [39]. The combined spectra around 711 cm^{-1} could also consist of the peak corresponding to the CaO content presented on the shells [38]. These surface functional groups of the adsorbent could potentially interact with Cu(II) and Zn(II) ions during its sorption onto the shell surface [40]. In addition, the peak approximately at 550 cm^{-1} corresponding to the presence of CuO structure was also observed in the UVS samples after being adsorbed by Cu(II) from aqueous solutions [41]. This formation of the CuO peak could be the result of cation exchange between Ca(II) and Cu(II) in the adsorption of Cu(II) ions onto the UVS active sites containing CaO structure. One important peak associated with the Zn(II) adsorption at around 500 cm^{-1} indicating the formation of ZnO [42] was not able to be seen from the experiment due to the limitation of the FTIR instrument in which it can be performed only at wavenumber in the range of 4000 to 550 cm^{-1}. It was believed that the ZnO bonding would be formed during the adsorption process of Zn(II), similar to the formation of CuO.

3.2. Copper and zinc speciation

Copper and zinc speciation as a function of pH was investigated according to the prediction results from MEDUSA® software [43]. The predominant diagrams of Cu(II) and Zn(II) in aqueous solutions under the studied conditions are illustrated in Figure 6. At a pH value of 7, the prediction results showed that copper speciation consisted of Cu^{2+}, $Cu(OH)^{+}$, and CuO as the predominant species. Whereas, zinc predominance containing Zn^{2+}, $ZnOH^{+}$, $Zn(OH)_2$, Zn_2OH^{3+}, and ZnO was presented in the prepared aqueous solution. The free copper and zinc cations theoretically compete for available active sites on the UVS surfaces [44], in which the adsorption kinetics of Cu(II) and Zn(II) will be later discussed. However, no precipitation was visually observed in all experiments under the operating conditions. It should be noted that the equilibrium models of the metal ions obtained from the software presumably consider only each aqueous Cu(II) and Zn(II) species and their corresponding homogeneous equilibria in the isolated environment. The

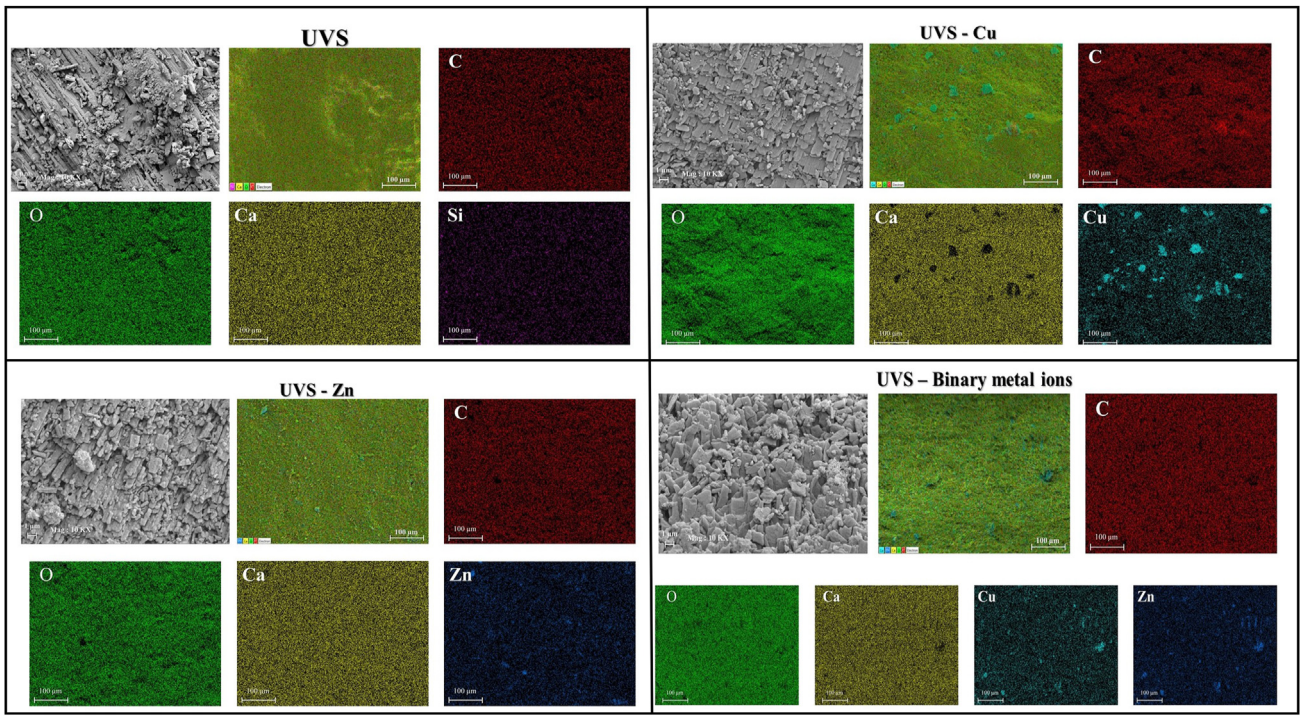

Figure 4. EDX elemental mapping results of unsued UVS (upper left), after being adsorbed with Cu(II) (upper right), after being adsorbed with Zn(II) (lower right), and after being adsorbed with binary Cu(II)/Zn(II) (lower right).

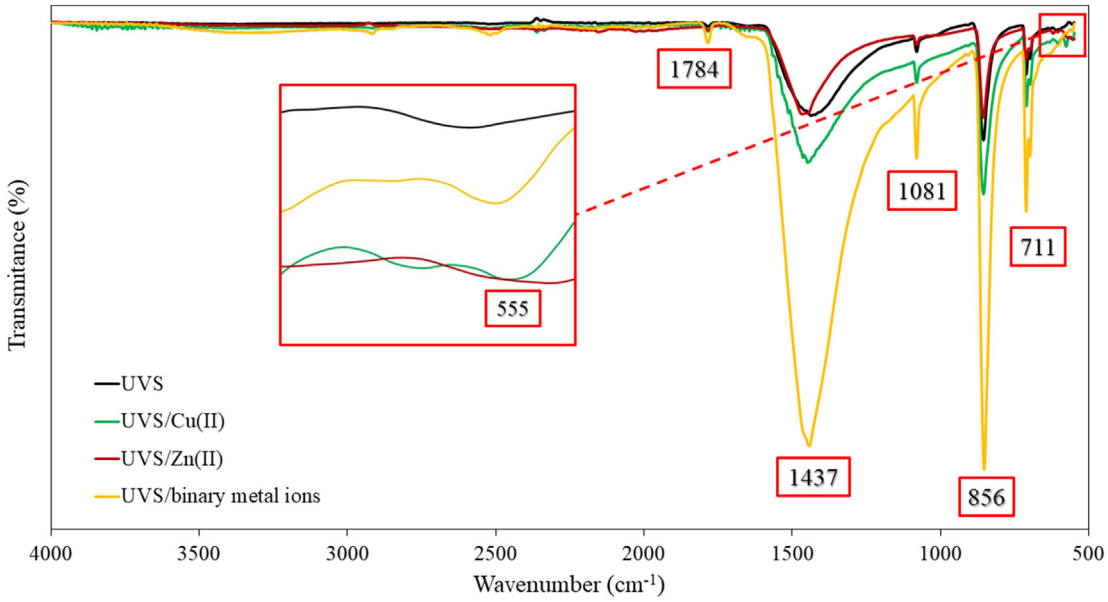

Figure 5. FTIR result of untreated Venus shells (UVS) before and after adsorption of Cu(II), Zn(II), and binary Cu(II)/Zn(II) using 100 g adsorbent at the initial metal ion concentration of 200 mg/L.

equilibria could be altered during the ongoing adsorption process due to decreasing in cation concentrations in the mixed Cu(II)/Zn(II) solution in the presence of the heterogeneous adsorbent.

3.3. Adsorption study

3.3.1. Effect of adsorbent dosages

The study of adsorbent dosages for removal of Cu(II) and Zn(II) was carried out at different shell dosages in a binary aqueous solution containing a concentration of 400 mg/L of Cu(II) and Zn(II) each. As illustrated in Figure 7, the amount of presented Cu(II) and Zn(II) in the solution in terms of C/C_0 decreased with increasing adsorption time. With decreasing C/C_0, the metal ions were adsorbed onto the active adsorbent surface. The result showed the adsorption rate increased when more amounts of adsorbent were used, and consistent with the other studies [38, 39]. At low dosages, the adsorption rate was relatively slow, and the process had not reached its equilibrium over the study period. With high dosages, both Cu(II) and Zn(II) were quickly adsorbed onto the shell, and the equilibrium had obtained, indicating the maximum adsorption capacity of the system. Increases in the percentage of metal

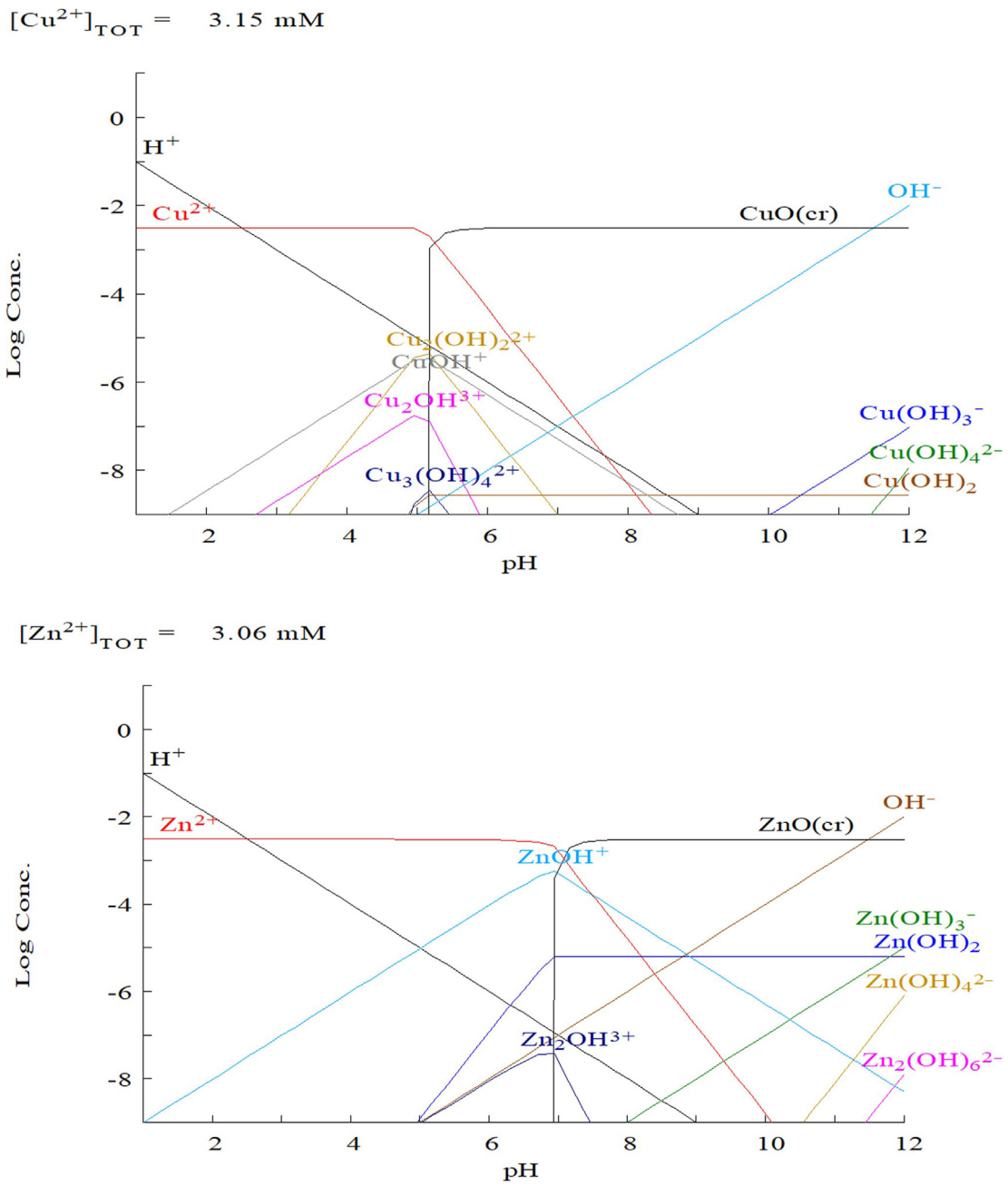

Figure 6. Prediction of copper (upper) and zinc (lower) speciations as a function of pH in an aqueous solution established using MEDUSA® software.

ions removal with UVC-600 dosages could be attributed to increases in the surface areas accordingly available for Cu(II) and Zn(II) adsorption [45].

3.3.2. *Effect of adsorbent size on adsorption efficiency*

The effect of adsorbent size on the adsorption efficiency of Cu(II) and Zn(II) ions was studied in a system containing UVS with various sizes (100 g each) in a mixed solution (250 mL) with each Cu(II) and Zn(II) concentration at 200 mg/L. The adsorption efficiency in terms of $1 - C/C_0$ was plotted over the adsorption period, as presented in Figure 8.

In the beginning, Cu(II) could be removed faster and in a larger amount than that of Zn(II) from the aqueous solution for all three different sizes of adsorbent. As seen from the figure, smaller size of adsorbent could adsorb more of Cu(II) and Zn(II) at the beginning period (up to 300 min), C/C_0 decreased rapidly during this period. This finding was consistent with the BET result examination. At a longer time (roughly more than 500 min), C/C_0 were roughly the same until the end of the experimental period. After the adsorption period, about 90 percent of Zn(II) was adsorbed onto the adsorbents, relatively higher than that of Cu(II) for all sizes. From the results, UVS-600 is the most suitable adsorbent since it gave good overall adsorption capacities for both Cu(II) and Zn(II). It was selected for further adsorption kinetics and Isotherm studies.

3.3.3. *Effect of initial concentration*

The effect of initial mixed concentrations of synthetic wastewater on the adsorption performance of UVS-600 is illustrated in Figure 9. The adsorption capacities of the shells trendily decreased when the initial concentration of Cu(II) and Zn(II) in mixed solution increased from 100 to 500 mg/L. At lower concentrations, there were sufficient active sites to adsorb the adsorbates when free Cu(II) and Zn(II) ions were able to adsorb onto the unoccupied sited throughout the adsorption process

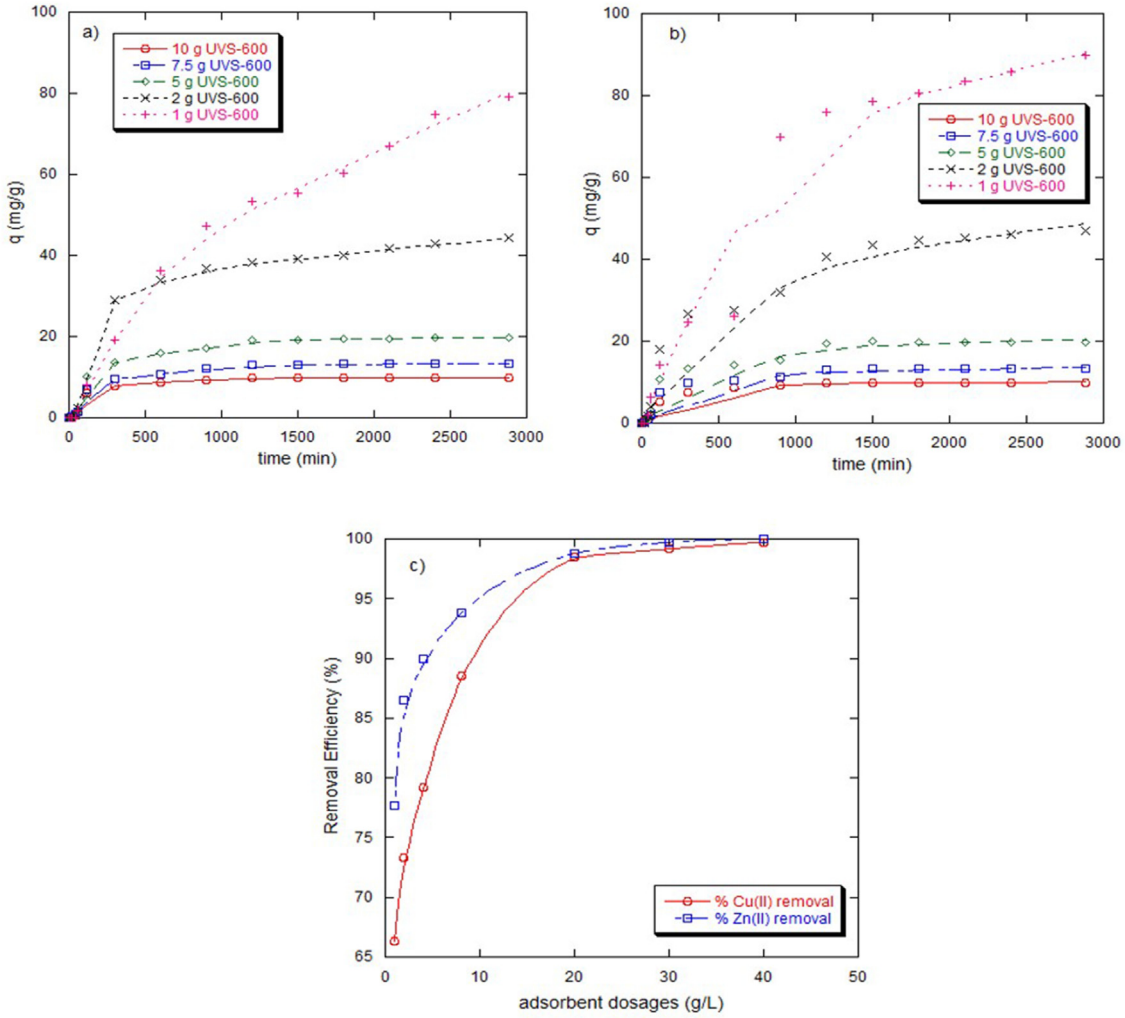

Figure 7. Effect of UVS-600 dosages on the ion concentration of a) Cu(II) and b) Z(II) in the aqueous solution and c) % removal efficiency of Cu(II) and d) Zn(II) adsorption.

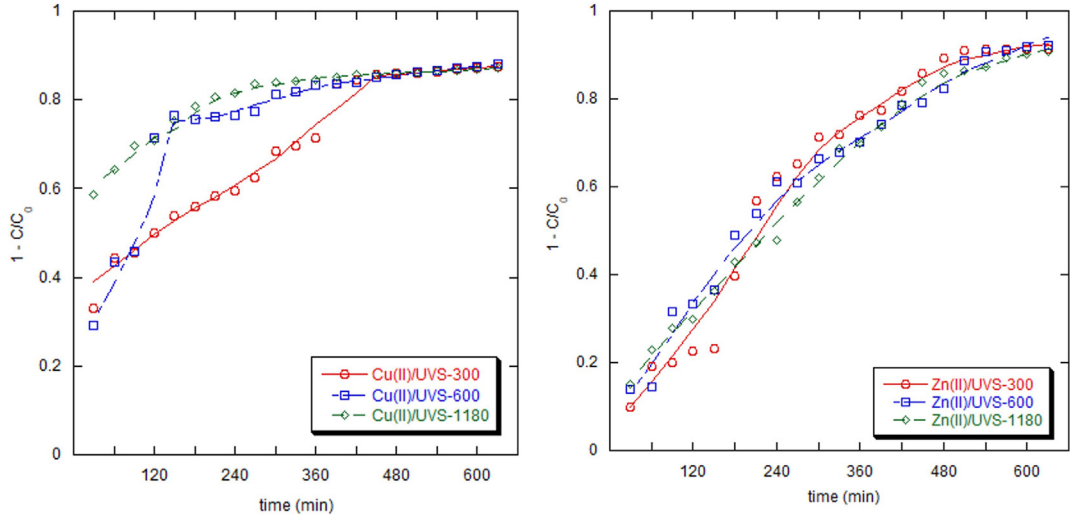

Figure 8. Effect of adsorbent size on adsorption efficiency of Cu(II) (left) and Zn(II) (right).

[46]. However, when the amount of the adsorbates in the solution increased, not all metal ions could be adsorbed onto the limited active sites of the adsorbent [47]. At high concentrations, the presence of Cu(II) and Zn(II) excess amounts could cause surface complications due to ionic interactions between the involved ions and the adsorbent surface that would affect the diffusion of the ions to the adsorption sites [48].

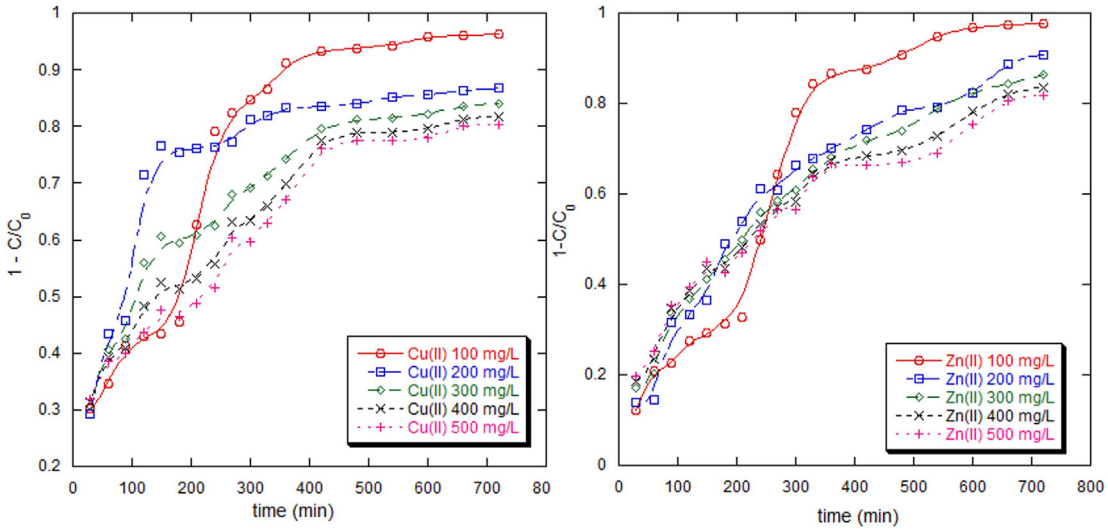

Figure 9. Effect of initial concentration on Cu(II) and Zn(II) adsorption onto UVS-600.

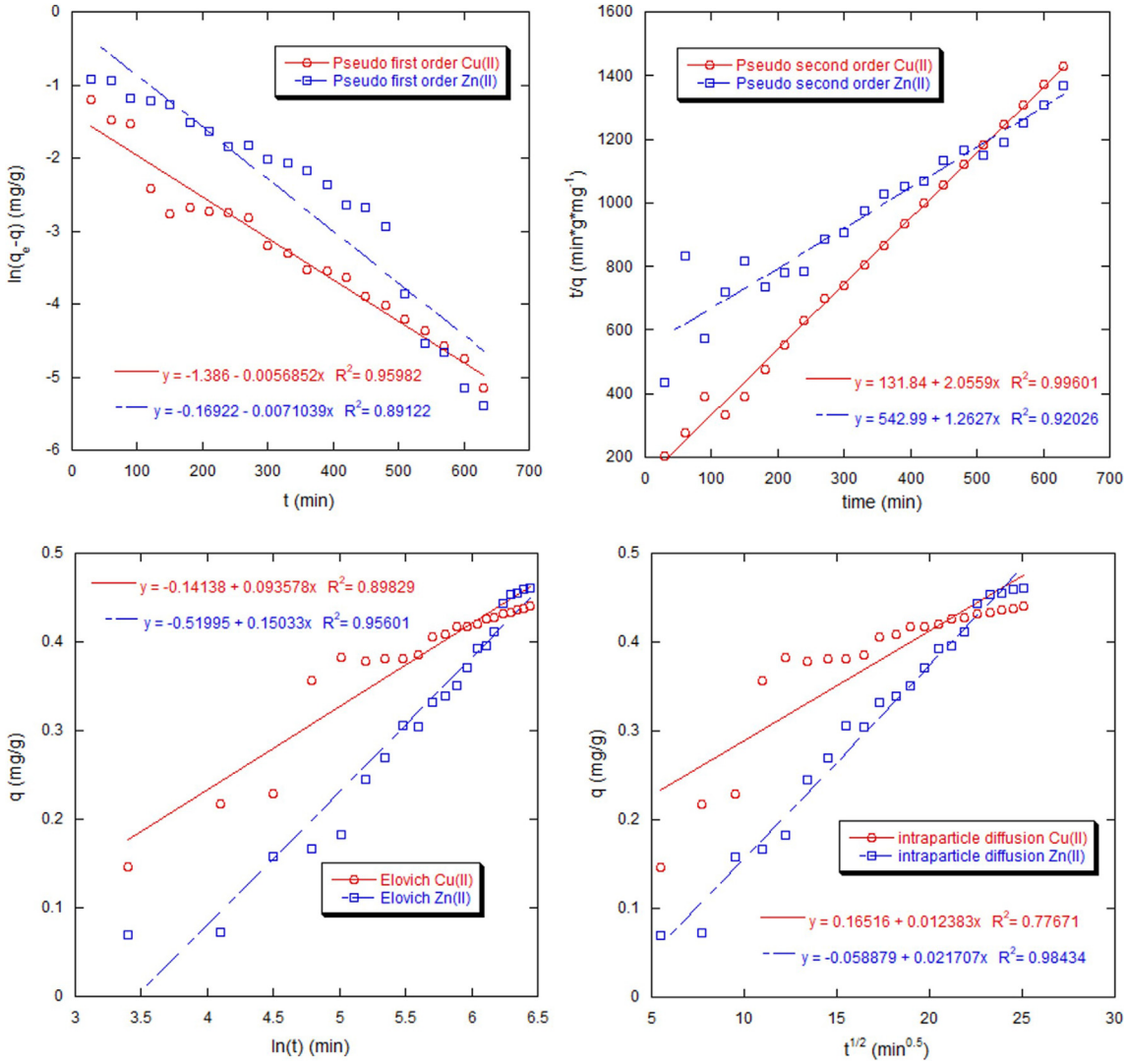

Figure 10. The linear regression analysis of kinetic models: pseudo-first order (upper left), pseudo-second order (upper right), Elovich (lower left), and intraparticle diffusion (lower right).

3.4. Adsorption study

3.4.1. Adsorption kinetics

During an adsorption process, the adsorbate would transport from bulk phase to hydrodynamic boundary layer around the adsorbent, then diffuse through the film boundary to the surface (film diffusion). The adsorbate molecules could further diffuse into the interior of the particles (interparticle diffusion). Finally, the adsorbate molecules are adsorbed onto the final adsorption sites, which depends on the energetic interactions between the paired molecules and sites [49]. In this study, pseudo-first order, pseudo-second order, Elovich, and intraparticle diffusion (IPD) models were investigated to get a better understanding of the adsorption process of binary Cu(II) and Zn(II) metal ions onto the shell adsorbents. Figure 10 illustrates the linear regression analysis of the studied kinetic models. Table 3 summarizes the analysis results for parameters of all applicable kinetic models mentioned above.

The pseudo-first order (PFO) model generally assumes that the adsorption capacity is a direct proportion to the difference between the concentration at any contact time and the equilibrium value, in which the occupation rate of adsorbent sites directly depends on the number of unoccupied sites. Thus, the pseudo-first order kinetic model was derived based on the assumption of physisorption control [50]. The linear form of pseudo-first order model is shown in Eq. (3), also known as the Lagergren equation [51].

$$\ln(q_e - q) = \ln(q_e) - k_1 t \tag{3}$$

where q_e (mg/g) is the amounts of metal ions adsorbed at equilibrium, and k_1 (min^{-1}) is the rate constant of pseudo-first order. The rate constant k_1 can be analyzed by a linear plot of $ln\ (q_e - q)$ against time. From Table 1, the experimental adsorption data showed a good fit to the PFO model with correlation coefficient (R^2) values of 0.9598 for Cu(II) and 0.8912 for Zn(II), respectively. However, the calculated q_e obtained from the analysis for Cu(II) (0.2545 mg/g) and for Zn (0.8443 mg/g) were lower than the experimental values for Cu(II) (0.4460 mg/g) and Zn(II) (0.465 mg/g). This suggested that the PFO model might not be applicable for the adsorption of both metal ions onto the shells.

The pseudo-second order (PSO) model was also applied for the adsorption kinetics analysis. The model assumes that chemisorption is the rate-determining step [51]. The linear form of the model is presented in Eq. (4), where k_2 is the equilibrium rate constant of pseudo-second order adsorption (g/mg/min). The values of q_e and k_2 were calculated from the slope and intercept of the linear plot of t/q against t. As reported in Table 1, the R^2 value of 0.9960 for the Cu(II) adsorption indicates that the pseudo-second order model provides almost a perfect fit to the experimental data. This result is in good agreement with other studies in which the Calcined golden apple snail shell [52] and Solamen Vaillant snail [53] were used as the biosorbents. In addition, the q_e (0.4864 mg/g) calculated from the PSO model was the closest to the experimental data (0.4460 mg/g). In the case of Zn(II), the pseudo-second order model also gave a reasonable fit with a lower R^2 value of 0.9203. Since the processes were likely to follow the pseudo-second order equation, it suggested that the adsorption was possibly the result of chemical interactions between the metal ion molecules and the surface functional groups on UVS adsorbent [33]. The presence of some carbonate groups on the shell surface might have been involved in bonding with the Cu(II) and Zn(II) ion molecules [54]. The finding was in good agreement with the FTIR analysis result.

$$\frac{t}{q} = \frac{1}{k_2 q_e^2} + \frac{1}{q_e} t \tag{4}$$

The Elovich model was applied to further investigate the assumption of chemisorption for the heterogeneous system, as illustrated in Eq. (5) [55]. The parameter α (mg/g.min) is the initial sorption rate, and β (g/mg) is the constant related to the surface coverage and activation energy of chemisorption in the Elovich model. As seen in Table 1, In Cu(II) adsorption, the model also did not fit well to the experimental result with a low R^2 value of 0.8983. On the other hand, a good fit of Zn(II) adsorption data was obtained with a higher R^2 value (0.9560). Thus, the Elovich model suggests the chemisorption might be significantly involved in Zn(II) but not for Cu(II) adsorption onto the shell surfaces.

Table 3. Adsorption kinetic parameters.

Kinetic models	Cu(II) adsorption	Zn(II) adsorption
Experimental q_e (mg/g)	0.446	0.465
Pseudo-first order (PFO)		
slope = $-k_1$	-0.0057	-0.0071
intercept = $\ln(q_e)$	-1.3686	-0.1692
Calculated k_1 (min^{-1})	0.0057	0.0071
Calculated q_e (mg/g)	0.2545	0.8443
R^2	0.9598	0.8912
Pseudo-second order (PSO)		
slope = $1/q_e$	2.0559	1.2627
intercept = $-1/k^2q_e^2$	131.84	542.99
k_2 (g/mg/min)	0.0321	0.0029
Calculated q_e (mg/g)	0.4864	0.7920
R^2	0.9960	0.9203
Elovich		
slope = 1/b	0.0936	0.1503
intercept	-0.1414	-0.5199
α (mg/g.min^{-1})	0.0207	0.0047
β (g/mg)	10.6838	6.6534
R^2	0.8983	0.9560
Intraparticle diffusion		
slope = k_{int}	0.0124	0.0217
intercept = C	0.1652	-0.0589
k_{int} (mg/g/min0.5)	0.0124	0.0217
C (mg/g)	0.1652	-0.0589
R^2	0.7767	0.9843

$$q = \frac{1}{\beta}\ln(\alpha\beta) + \frac{1}{\beta}\ln(t) \tag{5}$$

The experimental data were fitted to the intraparticle diffusion model to get a better understanding of the controlling step of the adsorption rate. The model is expressed in Eq. (6), where k_{int} (mg/g.min) is the intraparticle diffusion rate constant calculated from the slope of the plot q versus $t^{0.5}$. As shown in Table 1, the intraparticle model represents a very good fit for Zn(II) adsorption with a high R^2 value close to unity (0.9843). It suggests that the intraparticle diffusion mechanism could be strongly involved during the ongoing adsorption process of Zn(II). From Table 2, the linear regression analysis gave the intercept at which the plot of q versus $t^{0.5}$ did not pass through the origin. This implies that the intraparticle diffusion may not be the only rate-limiting step for the Zn(II) adsorption into the shell surface. In this case, film diffusion through some thickness of the boundary layer is also taking place [56]. However, the low R^2 value (0.7767) for Cu(II) adsorption indicates the invalidity of this model. The adsorption of Cu(II) ions onto the UVS adsorbent is unlikely to involve intraparticle diffusion inside the adsorbent particles. From the PSO analysis, Cu(II) ion molecules could be strongly adsorbed on the surface by chemisorption, accordingly observed in other related studies [47, 48, 49].

$$q = k_{int} t^{0.5} \tag{6}$$

3.4.2. Adsorption isotherms

In this study, the equilibrium data obtained from the adsorption processes of Cu(II) and Zn(II) onto UVC-600 (dosage of 100 g/250 mL solution) at 298 K from various initial concentrations were used to

analyze the equilibrium characteristics. The parameters of Langmuir, Freundlich, Temkin, and Dubinin - Radushkevich (D-R) isotherms were calculated by linear regression, while those of Langmuir-Freundlish (LF) isotherm was obtained by non-linear fitting. These parameters of equilibrium isotherms would give an insight into the sorption mechanism of adsorbed ions and their affinities towards the adsorbent [45]. The calculated adsorption parameters and the correlation coefficient obtained from linear regression (R^2) for the studied isotherms are summarized in Table 4.

The Langmuir isotherm is based on the homogeneous surface with identical active sites in which monolayer adsorption of the adsorbates onto the surface takes place without interactions between the adsorbed species [57]. The linearized form of the Langmuir equation is shown in Eq. (7), where q_m (mg/g) and b (L/mg) are the maximum monolayer adsorption capacity and adsorption energy, respectively. Both values were obtained from the slope and intercept of the plot between C_e and C_e/q_e. In general, high values of the correlation coefficient ($R^2 > 0.95$) indicate a good fit of the model. The correlation coefficient (R^2) of both Cu(II) and Zn(II) ions were 0.8946 and 0.9335, respectively, indicating that the monolayer Langmuir isotherm did not fit well to the adsorption of both metal ions onto UVC-600. Additionally, the essential characteristics of Langmuir isotherm were analyzed in terms of a separation or equilibrium parameter, as shown in Eq. (8). The R_L indicates the nature of adsorption: favorable isotherm ($0 < R_L < 1$), irreversible isotherm ($R_L = 0$), linear isotherm ($R_L = 1$), and unfavorable isotherm ($R_L > 1$) [58]. As seen in Figure 10, the separation factor (R_L) values were found to be less than unity at all initial concentrations for the adsorption of both metal ions. The higher the initial concentration, the isotherm becomes more favorable and irreversible as the R_L values decrease towards zero. Moreover, the adsorption behavior of Cu(II) and Zn(II) onto UVS-600 is related to surface coverage (θ) of the adsorbent, according to the result of their Langmuir isotherm analysis. The surface coverage (θ) is presented in Eq. (9), where K_L is Langmuir equilibrium adsorption constant. The surface coverage of the adsorbent particles increases with the increasing initial concentration of the metal ions (see Figure 11). As the used initial concentration increased to 500 mg/L, the surface coverage values reached more than 0.95 for both metal ions, indicating that most of the active sites on the surface were occupied by the adsorbed molecules and very few vacant sites left for adsorption.

$$\frac{C_e}{q_e} = \frac{1}{q_m b} + \frac{C_e}{q_m} \tag{7}$$

$$R_L = \frac{1}{1 + K_L C_0} \tag{8}$$

$$K_L C_0 = \frac{\theta}{1 - \theta} \tag{9}$$

The Freundlich isotherm model is applied based on multilayer adsorption on a heterogeneous surface [59]. The linearized form of the Freundlich equation is presented in Eq. (10), where K_F ((mg/g)(l/mg)$^{1/n}$) and n represent the adsorption capacity and adsorption effectiveness, respectively. Both constants were taken from the intercept and slope of the plot between $\log(q_e)$ and $\log(C_e)$. Compared with the Langmuir model, the adsorption of both metal ions was better fitted by the Freundlich isotherm with higher R^2 values of 0.9865 for Cu(II) and 0.9743 for Zn(II). The K_F values for Cu(II) and Zn(II) were 0.1724 and 0.1288 (mg/g) (L/mg)$^{1/n}$, respectively. While the n values were found to be 2.6674 (Cu(II) and 2.3474 (Zn(II)), indicating favorable adsorption ($1 < n < 10$) [60]. The results suggested easy separation and favorable adsorption of both metal ions onto the heterogeneous surface of the UVC-600 adsorbent. Comparing the K_F values for Cu (0.1724) and Zn (0.1288), the adsorption capacity of both metal ions onto the Venus shells was in the order Cu(II) > Zn(II). However, Cu(II) showed a better adsorption affinity towards the shell surfaces relative to the Zn(II) ions.

$$\log(q_e) = \log(K_F) + (1/n)\log(C_e) \tag{10}$$

The Temkin isotherm model, unlike the Langmuir and Freundlich isotherms, considers the interactions between adsorbents and metal ions to be adsorbed in which the model assumes that the free energy of sorption is a function of the surface coverage [3]. The interaction could cause a decrease in the heat of adsorption of all molecules in the layer linearly with increasing coverage [61]. The Temkin isotherm in a linear form is shown in Eq. (11), where B is a constant associated with the heat of adsorption, and A_T (L/mg) is a Temkin binding constant. From Table 2, the Temkin model did not well fit the experimental results with low correlation coefficient (R^2) values for both Cu(II) (0.8720) and Zn(II) (0.8976). The regression analysis gave the values of A_T (0.5831 L/mg for Cu(II) and 1.1246 L/mg for Zn(II) and b (11.50 kJ/mol for Cu(II) and 12.76 kJ/mol Zn(II)). Since the binding energy values were relatively high ($b < 8$ kJ/mol), chemisorption could take part in the adsorption of both metal ions to some extent [62].

$$q_e = B\ln(A_T) + B\ln(C_e) \tag{11}$$

The Dubinin-Radushkevich (D-R) isotherm is used to explain the adsorption process on a heterogeneous and porous surface with variable parameters [63]. Unlike Langmuir isotherm, the model does not assume a homogenous surface or a constant adsorption potential. The linear form of the D-R isotherm model is expressed in Eq. (12), where β is the coefficient related to adsorption energy (mol^2/J^2), q_m is the theoretical saturation capacity (mg/g), and ε is the Polanyi potential which is related to equilibrium concentration [64]. From Table 1, the D-R model gave a poor fit on the experimental data, having relatively low R^2 values (0.7226

Table 4. Parameters of adsorption isotherms.

Adsorption Isotherms	Cu(II) adsorption	Zn(II) adsorption
Langmuir		
slope = $1/q_m$	0.8275	0.8764
q_m (mg/g)	1.2085	1.1410
intercept = $1/q_m b$	25.7630	16.9630
b (L/mg)	0.0321	0.0517
R^2	0.8946	0.9335
Freundlich		
slope = 1/n	0.3749	0.4260
n	2.6674	2.3474
intercept = $\log(K_F)$	-0.7635	-0.8902
K_F (mg/g) (L/mg)1/n	0.1724	0.1288
R^2	0.9865	0.9743
Temkin		
slope = B	0.2154	0.1942
intercept = B*ln(A_T)	-0.1162	0.0228
b (kJ/mol)	11.5022	12.7578
A_T (L/mg)	0.5831	1.1246
R^2	0.8720	0.8976
Dubinin-Radushkevich (D-R)		
slope = -β	-1.1410	-2.7587
β	1.1410	2.7587
intercept = ln(q_m)	-0.4493	-0.4789
q_m (mg/g)	0.6381	0.6195
E (kJ/mol)	0.6620	0.4257
R^2	0.7226	0.7388
Elovich		
slope = -1/q_m	-2.2176	-2.8215
q_m (mg/g)	0.4509	0.3544
intercept = ln($K_e q_m$)	-2.6397	-1.9334
K_e (L/mg)	0.1583	0.4081
R^2	0.7827	0.8515

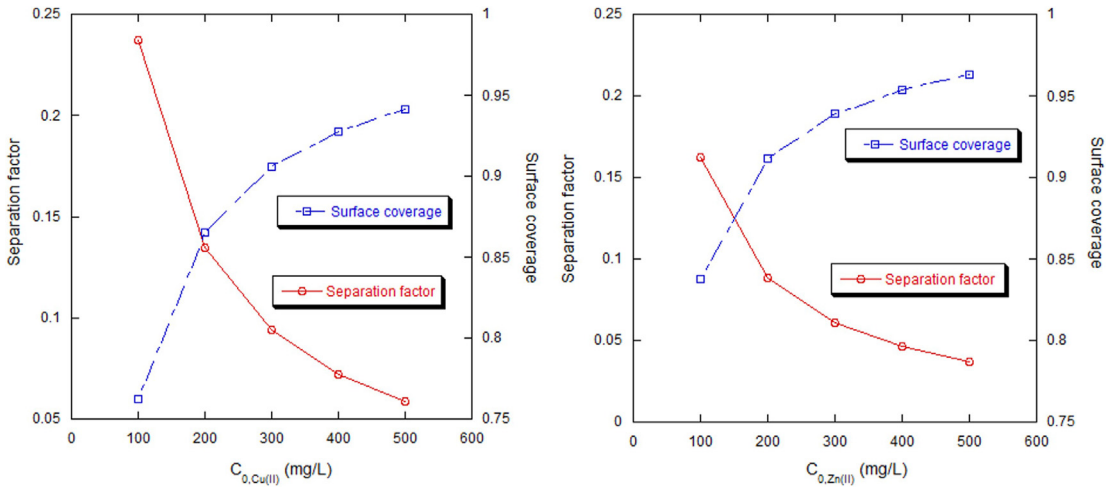

Figure 11. Effect of initial concentration on separation factor and surface coverage: Cu(II) adsorption (left), Zn(II) adsorption (right).

for Cu(II) and 0.7388) for Zn(II)) when compared with those of the other isotherms prior discussed.

$$\ln(q_e) = \ln(q_m) - \beta\varepsilon^2 \tag{12}$$

The Elovich isotherm assumes that adsorption sites increase exponentially with adsorption, implying multilayer adsorption [65]. The linear form of the model is given in Eq. (13), where q_m (mg/g) and K_e (L/mg) represent the adsorption capacity and the equilibrium constant [55]. The adsorption data did not fit well to the model with the R^2 values of 0.7827 for Cu(II) and 0.8515 for Zn(II). This implied that multilayer adsorption was unlikely to undertake in the adsorption of both metal ions in the studied concentration range.

$$\ln\left(\frac{q_e}{C_e}\right) = \ln(K_e q_m) - \frac{q_e}{q_m} \tag{13}$$

As summarized in Table 4, the Freundlich isotherm gave the best fit to the experimental data of binary Cu(II) and Zn(II) among the five tested isotherms. The results indicated that the adsorption of Cu(II) and Zn(II) onto UVS-600 adsorbent could probably undergo with chemisorption mechanism in which both metal ions from aqueous solution were competitively adsorbed onto the heterogenous of active sites available on the shell surfaces. The presence of both Cu(II) and Zn(II) ions in the binary system could result in ionic interference between the involving ions and the active sites, as reported on other multicomponent systems [71–73].

4. Conclusions

The possibility of UVS application as a bioadsorbent for the removal of metal ions in an aqueous solution was investigated. The major affecting parameters, including adsorbent dose, initial ion concentration, and adsorbent size, were studied. The maximum adsorption capacities of Cu(II) and Zn(II) were found to be 0.446 and 0.465 mg/g, respectively. From the kinetic data analysis, the adsorption of Cu(II) followed the pseudo-second order model, while the adsorption of Zn(II) followed the intraparticle diffusion model. The adsorption isotherm data revealed that the Freundlich model yielded the best fit to the equilibrium data for both Cu(II) and Zn(II) ions. The results indicated that the chemisorption of Cu(II) and Zn(II) onto UVS adsorbent could probably take place. Both metal ions in an aqueous solution were competitively adsorbed onto the heterogeneous of available active sites on the shell surfaces. The presence of both Cu(II) and Zn(II) ions in the binary system could result in ionic interference between the involving ions and the active sites, as reported on other multicomponent systems. Removal efficiencies of both metal ions using UVS adsorbent obtained in this study were relatively high (75–100%). Hence, it could be concluded that the UVS can be applied as an economical biosorbent for the treatment of heavy metals in aqueous solutions.

Declarations

Author contribution statement

Attaso Khamwichit, Wipawee Dechapanya: Conceived and designed the experiments; Performed the experiments; Analyzed and interpreted the data; Contributed reagents, materials, analysis tools or data; Wrote the paper.

Wipada Dechapanya: Analyzed and interpreted the data; Wrote the paper.

Funding statement

Wipawee Dechapanya was supported by Walailak University.

Data availability statement

Data included in article/supp. material/referenced in article.

Declaration of interest's statement

The authors declare no conflict of interest.

Additional information

No additional information is available for this paper.

Acknowledgements

This work was financially supported by Research Grant No. The funding grant number WUSTP-05/256, Walailak University, Thailand.

References

[1] H.A. Alalwan, M.A. Kadhom, A.H. Alminshid, Removal of heavy metals from wastewater using agricultural byproducts, J. Water Supply Res. Technol. - Aqua 69 (2) (Mar. 2020) 99–112.
[2] S.K. Gunatilake, Methods of removing heavy metals from industrial wastewater, J. Multidiscip. Eng. Sci. Stud. 1 (1) (Nov. 2015) 12–18.
[3] J. Wang, C. Chen, Biosorbents for heavy metals removal and their future, Biotechnol. Adv. 27 (2) (Mar. 2009) 195–226.
[4] N.R. Lynch, T.C. Hoang, T.E. O'Brien, Acute toxicity of binary-metal mixtures of copper, zinc, and nickel to *Pimephales promelas* : evidence of more-than-additive effect, Environ. Toxicol. Chem. 35 (2) (Feb. 2016) 446–457.

[5] M. Bilal, et al., Waste biomass adsorbents for copper removal from industrial wastewater—a review, J. Hazard Mater. 263 (Dec. 2013) 322–333.
[6] D.W. O'Connell, C. Birkinshaw, T.F. O'Dwyer, Heavy metal adsorbents prepared from the modification of cellulose: a review, Bioresour. Technol. 99 (15) (Oct. 2008) 6709–6724.
[7] N.A.A. Babarinde, J.O. Babalola, R.A. Sanni, Biosorption of lead ions from aqueous solution by maize leaf, Int. J. Phys. Sci. 1 (1) (Sep. 2006) 23–26.
[8] L.M. Plum, L. Rink, H. Hajo, The essential toxin: impact of zinc on human health, Int. J. Environ. Res. Publ. Health 7 (4) (2010) 1342–1365. MDPI.
[9] T.J. Porea, J.W. Belmont, J.D.H. Mahoney, Zinc-induced anemia and neutropenia in an adolescent, J. Pediatr. 136 (5) (May 2000) 688–690.
[10] S. Babel, T.A. Kurniawan, Low-cost adsorbents for heavy metals uptake from contaminated water: a review, J. Hazard Mater. 97 (1–3) (Feb. 2003) 219–243.
[11] S.M. Lee, C. Laldawngliana, D. Tiwari, Iron oxide nano-particles-immobilized-sand material in the treatment of Cu(II), Cd(II) and Pb(II) contaminated waste waters, Chem. Eng. J. 195–196 (Jul. 2012) 103–111.
[12] J.-C. Lee, Y.-O. Son, P. Pratheeshkumar, X. Shi, Oxidative stress and metal carcinogenesis, Free Radic. Biol. Med. 53 (4) (Aug. 2012) 742–757.
[13] S. Tamjidi, A. Ameri, A review of the application of sea material shells as low cost and effective bio-adsorbent for removal of heavy metals from wastewater, Environ. Sci. Pollut. Res. 27 (25) (Sep. 2020) 31105–31119.
[14] C. Nanthamathee, C. Chantarangkul, C. Jakkrawhad, A. Payaka, P. Dechatiwongse, Fine-tuning the dye adsorption capacity of UiO-66 by a mixed-ligand approach, Heliyon 8 (2) (Feb. 2022) e08961.
[15] U. Jinendra, D. Bilehal, B.M. Nagabhushana, A.P. Kumar, Adsorptive removal of Rhodamine B dye from aqueous solution by using graphene–based nickel nanocomposite, Heliyon 7 (4) (Apr. 2021).
[16] F. Ahmad, S. Zaidi, Potential use of agro/food wastes as biosorbents in the removal of heavy metals, in: Emerging Contaminants, IntechOpen, 2021.
[17] S.T. Akar, et al., Removal of copper(II) ions from synthetic solution and real wastewater by the combined action of dried Trametes versicolor cells and montmorillonite, Hydrometallurgy 97 (1–2) (Jun. 2009) 98–104.
[18] H.S. Mohamed, et al., Adsorption of Cd 2D and Cr 3D ions from aqueous solutions by using residue of Padina gymnospora waste as promising low-cost adsorbent, Heliyon 5 (2019) 1287.
[19] W. Dechapanya, S. Rattanahirun, A. Khamwichit, Syngas production from palm kernel shells with enhanced tar removal using biochar from agricultural residues†, Front. Energy Res. 8 (Jul) (2020).
[20] L. Massimi, A. Giuliano, M. Astolfi, R. Congedo, A. Masotti, S. Canepari, Efficiency evaluation of food waste materials for the removal of metals and metalloids from complex multi-element solutions, Materials (Basel) 11 (3) (Feb. 2018) 334.
[21] N. Basci, E. Kocadagistan, B. Kocadagistan, Biosorption of copper (II) from aqueous solutions by wheat shell, Desalination 164 (2) (Apr. 2004) 135–140.
[22] K. Wong, C. Lee, K. Low, M. Haron, Removal of Cu and Pb by tartaric acid modified rice husk from aqueous solutions, Chemosphere 50 (1) (Jan. 2003) 23–28.
[23] J.C. Moreno-Piraján, L. Giraldo, Activated carbon obtained by pyrolysis of potato peel for the removal of heavy metal copper (II) from aqueous solutions, J. Anal. Appl. Pyrolysis 90 (1) (Jan. 2011) 42–47.
[24] S.B. Choi, Y.-S. Yun, Lead biosorption by waste biomass of Corynebacterium glutamicum generated from lysine fermentation process, Biotechnol. Lett. 26 (4) (Feb. 2004) 331–336.
[25] M. Mohammad, S. Maitra, N. Ahmad, A. Bustam, T.K. Sen, B.K. Dutta, Metal ion removal from aqueous solution using physic seed hull, J. Hazard Mater. 179 (1–3) (Jul. 2010) 363–372.
[26] M. Iqbal, A. Saeed, I. Kalim, Characterization of adsorptive capacity and investigation of mechanism of Cu $^{2+}$, Ni $^{2+}$ and Zn $^{2+}$ adsorption on mango peel waste from constituted metal solution and genuine electroplating effluent, Separ. Sci. Technol. 44 (15) (Oct. 2009) 3770–3791.
[27] H.T. Van, et al., Characteristics and mechanisms of cadmium adsorption onto biogenic aragonite shells-derived biosorbent: batch and column studies, J. Environ. Manag. 241 (Jul. 2019) 535–548.
[28] B. Zhao, J.E. Zhang, W. Yan, X. Kang, C. Cheng, Y. Ouyang, Removal of cadmium from aqueous solution using waste shells of golden apple snail, New Pub. Balaban 57 (50) (Oct. 2016) 23987–24003.
[29] D. Alidoust, M. Kawahigashi, S. Yoshizawa, H. Sumida, M. Watanabe, Mechanism of cadmium biosorption from aqueous solutions using calcined oyster shells, J. Environ. Manag. 150 (Mar. 2015) 103–110.
[30] Y. Du, F. Lian, L. Zhu, Biosorption of divalent Pb, Cd and Zn on aragonite and calcite mollusk shells, Environ. Pollut. 159 (7) (Jul. 2011) 1763–1768.
[31] S. Wang, H. Wu, Environmental-benign utilisation of fly ash as low-cost adsorbents, J. Hazard Mater. 136 (3) (Aug. 2006) 482–501.
[32] S. De Gisi, G. Lofrano, M. Grassi, M. Notarnicola, Characteristics and adsorption capacities of low-cost sorbents for wastewater treatment: a review, Sustain. Mater. Technol. 9 (Sep. 2016) 10–40.
[33] A.-H. Chen, S.-C. Liu, C.-Y. Chen, C.-Y. Chen, Comparative adsorption of Cu(II), Zn(II), and Pb(II) ions in aqueous solution on the crosslinked chitosan with epichlorohydrin, J. Hazard Mater. 154 (1–3) (Jun. 2008) 184–191.
[34] A.M. Alasadi, F.I. Khaili, A.M. Awwad, Adsorption of Cu(II), Ni(II) and Zn(II) ions by nano kaolinite: thermodynamics and kinetics studies, Chem. Int. (2019) 258–268.
[35] F.A. Dawodu, K.G. Akpomie, Simultaneous adsorption of Ni(II) and Mn(II) ions from aqueous solution unto a Nigerian kaolinite clay, J. Mater. Res. Technol. 3 (2) (Apr. 2014) 129–141.
[36] X.H. Vu, et al., Adsorption of chromium(VI) onto freshwater snail shell-derived biosorbent from aqueous solutions: equilibrium, kinetics, and thermodynamics, J. Chem. 2019 (Sep. 2019) 1–11.
[37] F.A. Ismail, A.Z. Aris, P.A. Latif, Dynamic behaviour of Cd2+ adsorption in equilibrium batch studies by CaCO3 −-rich Corbicula fluminea shell, Environ. Sci. Pollut. Res. 21 (1) (Jan. 2014) 344–354.
[38] E. Ferraz, J.A.F. Gamelas, J. Coroado, C. Monteiro, F. Rocha, Recycling waste seashells to produce calcitic lime: characterization and wet slaking reactivity, Waste Biomass Valorizat. 10 (8) (Aug. 2019) 2397–2414.
[39] M.D. Khan, T. Chottitisupawong, H.H.T. Vu, J.W. Ahn, G.M. Kim, Removal of phosphorus from an aqueous solution by nanocalcium hydroxide derived from waste bivalve seashells: mechanism and kinetics, ACS Omega 5 (21) (Jun. 2020) 12290–12301.
[40] C. Mahendra, R.R. Sivakiran, K.A. Badrinarayana, L. Priya, S. Raj, M. Mamatha, Investigation of bivalve molluscan seashells for the removal of cadmium, lead and zinc metal IONS from wastewater streams, Rasayan J. Chem. 12 (2) (2020) 903–914.
[41] T. Wang, D. Wang, H. Zhang, X. Wang, M. Chen, Laser-induced convenient synthesis of porous Cu_2O@CuO nanocomposites with excellent adsorption of methyl blue solution, Opt. Mater. Express 7 (3) (Mar. 2017) 924.
[42] G. Xiong, U. Pal, J.G. Serrano, K.B. Ucer, R.T. Williams, Photoluminesence and FTIR study of ZnO nanoparticles: the impurity and defect perspective, Phys. Status Solidi. 3 (10) (Nov. 2006) 3577–3581.
[43] I. Puigdomenech, Hydra/Medusa Chemical Equilibrium Database and Plotting Software, KTH Royal Institute of Technology, 2004 [Online]. Available: https://www.kth.se/che/medusa/downloads-1.386254. (Accessed 28 February 2022).
[44] C. Pennesi, et al., Adsorption of indium by waste biomass of brown alga Ascophyllum nodosum, Sci. Rep. 9 (1) (Dec. 2019).
[45] J.C.P. Vaghetti, et al., Application of Brazilian-pine fruit coat as a biosorbent to removal of Cr(VI) from aqueous solution-Kinetics and equilibrium study, Biochem. Eng. J. 42 (1) (Oct. 2008) 67–76.
[46] H. Radnia, A.A. Ghoreyshi, H. Younesi, G.D. Najafpour, Adsorption of Fe(II) ions from aqueous phase by chitosan adsorbent: equilibrium, kinetic, and thermodynamic studies, Desalinat. Water Treat. 50 (1–3) (2012) 348–359.
[47] F.Y. Wang, H. Wang, J.W. Ma, Adsorption of cadmium (II) ions from aqueous solution by a new low-cost adsorbent-Bamboo charcoal, J. Hazard Mater. 177 (1–3) (May 2010) 300–306.
[48] J.P. Chen, L. Hong, S. Wu, L. Wang, Elucidation of interactions between metal ions and Ca alginate-based ion-exchange resin by spectroscopic analysis and modeling simulation, Langmuir 18 (24) (Nov. 2002) 9413–9421.
[49] E.I. Unuabonah, M.O. Omorogie, N.A. Oladoja, Modeling in adsorption: fundamentals and applications, in: Composite Nanoadsorbents, Elsevier, 2018, pp. 85–118.
[50] A. Dutta, Y. Diao, R. Jain, E.R. Rene, S. Dutta, Adsorption of cadmium from aqueous solutions onto coffee grounds and wheat straw: equilibrium and kinetic study, J. Environ. Eng. 142 (9) (Sep. 2016).
[51] Y.S. Ho, G. Mckay, Pseudo-second Order Model for Sorption Processes, 1999.
[52] H. Esmaeili, S. Tamjidi, M. Abed, Removal of Cu(II), Co(II) and Pb(II) from synthetic and real wastewater using calcified Solamen Vaillanti snail shell, Desalin. Water Treat. 174 (2020) 324–335.
[53] C. Ketwong, S. Trisupakitti, C. Nausri, W. Senajuk, Removal OF heavy metal from synthetic waste water using calcined golden apple snail shells, Naresuan Univ. J. Sci. Technol. 26 (4) (Nov. 2018) 61–70.
[54] F. Dhaouadi, et al., Adsorption mechanism of Zn2+, Ni2+, Cd2+, and Cu2+ ions by carbon-based adsorbents: interpretation of the adsorption isotherms via physical modelling, Environ. Sci. Pollut. Res. 28 (24) (Jun. 2021) 30943–30954.
[55] F.C. Wu, R.L. Tseng, R.S. Juang, Characteristics of Elovich equation used for the analysis of adsorption kinetics in dye-chitosan systems, Chem. Eng. J. 150 (2–3) (Aug. 2009) 366–373.
[56] S. Nethaji, A. Sivasamy, A.B. Mandal, Adsorption isotherms, kinetics and mechanism for the adsorption of cationic and anionic dyes onto carbonaceous particles prepared from Juglans regia shell biomass, Int. J. Environ. Sci. Technol. 10 (2) (Mar. 2013) 231–242.
[57] I. Langmuir, The adsorption of gases on plane surfaces of glass, mica and platinum, J. Am. Chem. Soc. 40 (9) (Sep. 1918) 1361–1403.
[58] P. Baskaralingam, M. Pulikesi, D. Elango, V. Ramamurthi, S. Sivanesan, Adsorption of acid dye onto organobentonite, J. Hazard Mater. 128 (2–3) (Feb. 2006) 138–144.
[59] W. Clayton, Capillary and colloid chemistry, J. Soc. Chem. Ind. 45 (44) (Oct. 1926) 797–798. By Prof. H. Freundlich. Translated by H. Stafford Hatfield, B.Sc., Ph.D pp. xv+883. London: Methuen and Co., Ltd., 1926. Price: 50s.
[60] R.L. Tseng, F.C. Wu, Inferring the favorable adsorption level and the concurrent multi-stage process with the Freundlich constant, J. Hazard Mater. 155 (1–2) (Jun. 2008) 277–287.
[61] A.A. Inyinbor, F.A. Adekola, G.A. Olatunji, Kinetics, isotherms and thermodynamic modeling of liquid phase adsorption of Rhodamine B dye onto Raphia hookerie fruit epicarp, Water Resour. Ind. 15 (Sep. 2016) 14–27.
[62] N. Ayawei, A.N. Ebelegi, D. Wankasi, Modelling and interpretation of adsorption isotherms, J. Chem. 2017 (2017). Hindawi Limited.
[63] Q. Hu, Z. Zhang, Application of Dubinin–Radushkevich isotherm model at the solid/solution interface: a theoretical analysis, J. Mol. Liq. 277 (Mar. 2019) 646–648.
[64] M. Dubinin, E. Zaverina, L. Radushkevic, Sorption and structure of active carbons I. Adsorption of organic vapors, Zh. Fiz. Khim. 21 (1947) 1351–1362.
[65] M. Gubernak, W. Zapala, K. Kacmarski, Lysis of amylbenzene adsorption equilibria on an RP-18e chromatographic column, Acta Chromatogr. (23) (2003) 38–59.